Plasmon induced transparency in metal–insulator–metal waveguide by a stub coupled with F-P resonator

2014 Mater. Res. Express 1 036201

(http://iopscience.iop.org/2053-1591/1/3/036201)

Materials Research
Express

Plasmon induced transparency in metal–insulator–metal waveguide by a stub coupled with F-P resonator

Binfeng Yun, Guohua Hu, Cong Jiawei and Yiping Cui[1]
Advanced Photonics Center, Southeast University, Nanjing 210096, People's Republic of China
E-mail: ybf@seu.edu.cn, photonics@seu.edu.cn, roycia@163.com and cyp@seu.edu.cn.

Received 13 February 2014, revised 5 May 2014
Accepted for publication 16 June 2014
Published 1 July 2014
Materials Research Express **1** (2014) 036201
doi:10.1088/2053-1591/1/3/036201

Abstract
A simple and compact metal–insulator–metal (MIM) stub coupled with Fabry–Perot (FP) resonator is proposed to realize the plasmonic analogue of electromagnetically induced transparency. By the coupling between the stub and the FP resonator, a narrow transmission peak is formed in the broad stop-band of the stub resonator. By combining the magnetic field distributions and the plasmon hybridization theory, the physical mechanism is presented, which is the mode splitting caused by the evanescent coupling between the plasmonic resonators. And the effects of the structure parameters on the transmission characteristics of the coupled system are analyzed in detail. Also, double plasmon induced transmission peaks can be realized by simply adding a second FP resonator into the system. The proposed compact and simple plasmonic structure may have potential applications in nanoscale filter and slow-light devices.

Keywords: surface plasmons, plasmon induced transparency, metal-insulator-metal waveguides

1. Introduction

Surface plasmon polaritons (SPPs) are electromagnetic waves coherently coupled to electron oscillations which propagate at the interface between a dielectric and a metal, with evanescently decaying fields in both sides [1]. By combing the surface bonding SPPs at two metal/dielectric interfaces, a very compact metal–insulator–metal (MIM) waveguide can be realized, which can overcome the diffraction limit in dielectric waveguides and squeeze the mode size down to a few tens of nanometers [2]. Electromagnetically induced transparency (EIT) is a phenomenon

[1] Author to whom any correspondence should be addressed.

that occurs in atomic systems as a result of quantum interference between the atomic resonances [3], making the experimental realization of it rather challenging. By using the optical waveguide devices, the classical EIT-like transmission in atomic system can be easily realized, which can introduce novel functionalities into integrated optical circuits. And several optical analogues of EIT configurations with dielectric waveguides have been proposed and analyzed [4–6]. However, they have large footprints of hundreds of square microns due to the native diffraction limit, which has a limitation in high density integration. By using the nanoscale MIM plasmonic waveguides, very compact plasmon induced transparency (PIT) configurations which are a plasmonic analogue of the EIT can be realized. Recently, a number of PIT structures have been proposed, such as metal nano-particle coupled dielectric waveguides [7, 8], multiple MIM stub interferences [9–12], and coupled plasmonic FP resonators [13–15]. The PIT system based on the metal nano-particle coupled dielectric waveguides is difficult to fabricate because it needs to precisely put nano-particle close to the dielectric waveguide. The structures of the PIT system based on MIM stub interferences are simple but their transmission characteristics depend on the relative phase between them. The MIM stub is the most compact and simplest band-stop filter [16, 17], and by filling graded cascading MIM stubs with Kerr medium, Wang *et al* demonstrated a wide-band plasmonic optical switch with femtosecond-scale response time [18]. Cui *et al* proposed a compact PIT system by using the evanescent coupling between a MIM stub and a MIM ring resonator [19]. But the MIM ring structure is relative complex and difficult to fabricate precisely. The MIM FP resonator [20, 21] is a much simpler plasmonic filter structure comparing to the MIM ring resonator. Here we propose a very simple and compact PIT system which combines the MIM stub and the MIM FP resonator by direct evanescent coupling effect. To date almost all the PIT systems focused on the single PIT; multiple PIT structures have seldom been reported. Recently Chen *et al* proposed multiple PIT system based on the interferences among multiple MIM stubs [22]. Also, by introducing a second MIM FP resonator into our proposed PIT system, double plasmon induced transparencies can be easily formed. By using the FDTD and the plasmon hybridization model, the physical mechanism of the PIT phenomenon of the proposed PIT system is presented, which is the mode splitting caused by the evanescent coupling between the plasmonic resonators. Also, the effects of the structure parameters (such as stub size, FP resonator size, coupling gap size) on the transmission characteristics of the coupled system are analyzed in detail.

2. PIT in stub coupled with FP resonator system

The structure of the proposed PIT system which includes a MIM stub coupled with a MIM FP resonator head to head is shown in figure 1(a), where L, d, g and w denote the length of the FP resonator, the length of the stub, the couple gap size and the width of the MIM waveguide, respectively. The whole structure are based on the nanometric MIM waveguide and only the fundamental TM mode is supported, whose dispersion relation is given as [15]:

$$\varepsilon_{\text{in}} k_{z2} + \varepsilon_m k_{z1} \coth\left(-\frac{ik_{z1}}{2} w\right) = 0 \tag{1}$$

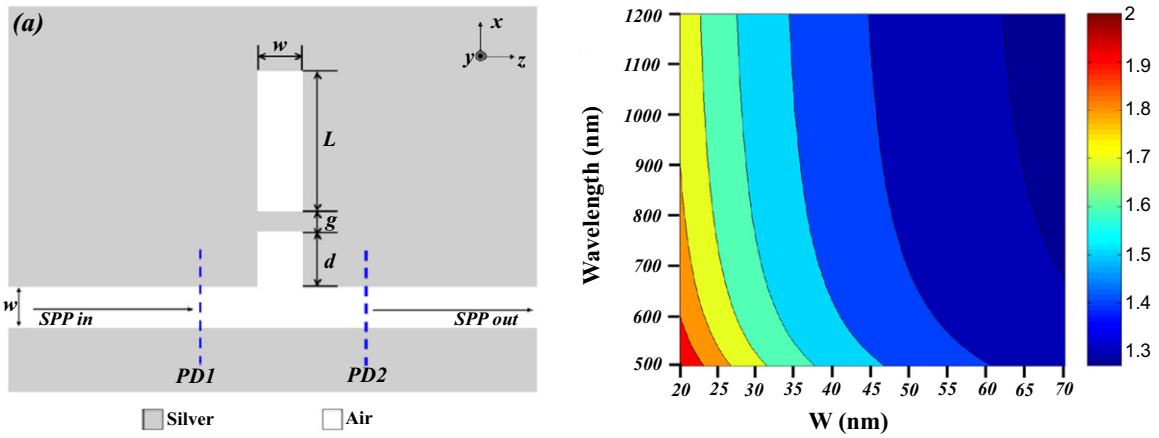

Figure 1. (a) The structure of the PIT system with MIM stub coupled with MIM FP resonator. (b) The dependence of Re(neff) of the fundamental TM mode on the wavelength of incident light λ and the width w.

and k_{z1} and k_{z2} are

$$k_{z1}^2 = \varepsilon_{\text{in}} k_0^2 - \beta^2, \quad k_{z2}^2 = \varepsilon_m k_0^2 - \beta^2 \tag{2}$$

where ε_{in}, ε_m are the dielectric constants of the insulator and the metal, $k_0 = 2\pi/\lambda$ is the free space wave vector. Here we choose silver as the metal and the air as the insulator and the dielectric constant of the silver is characterized by the well known Drude model [16]:

$$\varepsilon_m(\omega) = \varepsilon_\infty - \omega_p^2 / \omega(\omega + i\omega) \tag{3}$$

where $\varepsilon_\infty = 1.38 \times 10^{16}$ Hz is the bulk plasma frequency, which represents the nature frequency of the oscillations of free conduction electrons, $\gamma = 2.73 \times 10^{13}$ Hz is the damping frequency of the oscillations, ω is the angular frequency of the incident light, and $\varepsilon_\infty = 3.7$ is the dielectric constant at infinite angular frequency. And the real part of the effective index of the fundamental TM mode $\left(n_{\text{eff}} = \beta/k\right)$ as a function of slit width w and incident light wavelength λ is shown in figure 1(b). The results show the n_{eff} decreases as w increases and decreases relatively slow with increasing λ.

The proposed PIT nanostructure is simulated by using the 2D FDTD method with perfect matched layer boundary condition, where the fundamental TM mode is excited by a pulse source and the mesh grid size (Δx, Δy and Δz) used in FDTD simulation is set to 1 nm in order to keep convergence. Two monitors PD1 and PD2 are set to detect the incident power A_1 (without the stub and FP resonators for reference) and the transmission power A_2 (with the coupled stub and the FP resonators). The transmittance is defined as $T = A_2/A_1$.

The transmission spectra of the individual MIM FP resonator ($L = 500$ nm, $w = 50$ nm, $g = 10$ nm) and MIM stub resonator ($d = 100$ nm, $w = 50$ nm) are shown in figure 2(a). It is obvious that both resonators are band-stop filters and the rejection band of the MIM FP resonator is much narrower than that of the MIM stub resonator. It is because the coupling coefficient is much larger for the stub directly connected to the input MIM waveguide, while the MIM FP resonator is evanescent coupled to the input MIM waveguide with 10 nm gap. The field distributions of the magnetic component H_y at resonances for the MIM FP and MIM stub resonators are shown in figure 2(b) and figure 2(c), respectively. The stop bands of the MIM FP

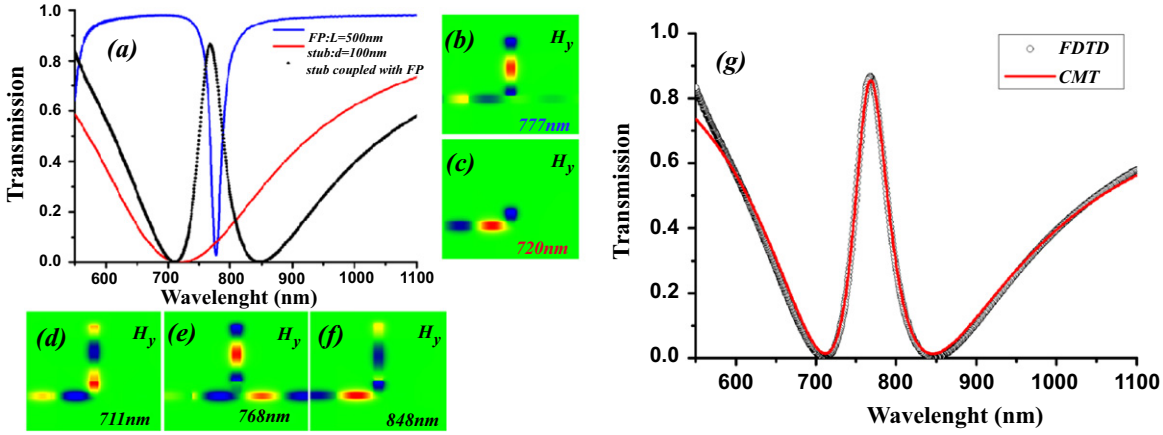

Figure 2. (a) The transmission spectra of the individual MIM FP resonator (blue line), stub (red line) and coupled PIT system (black dot); (b) The H_y field distribution of the MIM FP resonator at the resonance; (c) The H_y field distribution of the MIM stub resonator at the resonance; (d)–(f) The H_y field distributions of the coupled PIT system at resonant dips and peak. (g) The transmission spectra of the coupled PIT system calculated by the CMT (circles) and FDTD (red line).

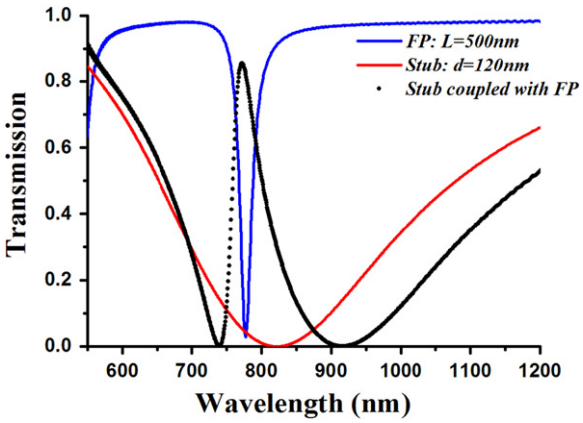

Figure 3. The transmission spectra of the individual MIM FP resonator (blue line), stub (red line) and coupled PIT system (black dot).

resonator and the MIM stub resonator are overlapped and when the two plasmonic resonators are evanescent coupled with a gap g as shown in figure 1(a), a PIT peak can be formed in the relative broad stop band of the MIM stub resonator, which is shown in figure 2(a). In other words, the broad resonant mode of the MIM stub is splitted into two resonant modes, one of them is blue shifted relative to the individual resonator while the other is red shifted, which can be clearly seen in the transmission spectrum of for the coupled system in figure 3 with MIM FP cavity length $L = 500$ nm and MIM stub size $d = 120$ nm, respectively. This phenomena is similar to the mode splitting according to the plasmon hybridization theory, which is used in the coupled metal nano-particle systems [23]. From the H_y field distributions of the two split resonances, which is shown in figure 2(d) and figure 2(f), it should be noted that for the split high energy mode, the H_y fields in the coupled cavities are inphase while the H_y fields are antiphase for the low energy mode. Besides, H_y fields are well coupled into the stub resonator

and antiphase with respect to the H_y fields in input MIM waveguides, which induce the destructive interference and transmission suppression. While for the PIT peak, the H_y fields shown in figure 2(e) indicate that the stub resonator is poorly coupled and oscillates inphase with the input MIM waveguide, which induces the PIT phenomenon. In order to validate our FDTD results, a temporal coupled mode theory (CMT) was used to analyze the transmission characteristics of the proposed PIT system. The transmission T of the output port can be expressed as [14]:

$$T = \left| \frac{j\left(\frac{\omega}{\omega_0} - 1\right) + \frac{1}{Q_i} - \frac{1}{2Q_1} + \frac{1}{Q_1}\frac{1}{1 - \sigma e^{-j\varphi}}}{j\left(\frac{\omega}{\omega_0} - 1\right) + \frac{1}{Q_i} - \frac{1}{2Q_1} + \frac{1}{2Q_2} + \frac{1}{Q_1}\frac{1}{1 - \sigma e^{-j\varphi}}} \right|^2 \tag{4}$$

Where ω_0 is the resonant frequepncy of the cavity, Q_i is the quality factor due to the intrinsic loss in the cavity and Q_1 and Q_2 are the quality factors related to the decay rate into the resonant and bus waveguides, respectively. Here φ and σ are the phase shift and attenuation terms of the SPP mode during a round trip in the resonator cavity, respectively. And the phase term φ can be described as:

$$\varphi(\omega) = \frac{\omega \,\mathrm{Re}(n_{\mathrm{eff}})\, L}{c} + \theta \tag{5}$$

Where n_{eff} and θ are the effective SPP mode index in resonant cavity and reflective phase shift on a metal facet. Figure 2(g) shows the transmission spectra of the coupled PIT system obtained by the FDTD and CMT method, where the FDTD result can be well fitted by the theoretical CMT model with assumed parameters $Q_i = 38$, $Q_1 = 23.5$, $Q_2 = 2.3$, $\omega_0 = 2.4229 \times 10^{15}$ rad s^{-1}, $L = 500$ nm, $\theta = 0.558$, and $\sigma = 0.984$, respectively.

It is well known that PIT phenomenon can be utilized to realize slow light effect [24]. Recently a plasmonic 'rainbow trapping' phenomenon has been reported by using the graded MIM stub grating structures [25]. Here the slow light effect of the proposed PIT system has also been investigated. The slow light effect can be described by the group index n_g, which can be expressed as [24]

$$n_g = \frac{c}{D} \times \frac{\mathrm{d}\phi(\omega)}{\mathrm{d}\omega} \tag{6}$$

Where c, D, ϕ, ω are the light speed in vacuum, length of the PIT system, transmission phase shift of the PIT system and angular frequency, respectively. The simulated transmission phase shift and group indices of the proposed PIT system are shown in figure 4(a) and figure 4(b), respectively. It is obvious that the group index is greatly increased around the PIT peak due to the strong dispersion in the transmission window. The maximum group index is about 37, which is comparable with those obtained in [24, 25].

As is known, the transmission characteristics of the coupled PIT system can be affected by the structure parameters. First, the effects of the coupling gap size g on the PIT spectra are investigated and are shown in figure 5. It is obvious that the energy gap between two split resonant modes gets larger when the coupling gap size g between the MIM FP resonator and MIM stub decreases. This can be explained by the plasmon hybridization theory that the interactions between the MIM FP and stub resonators get stronger with decreasing coupling gap

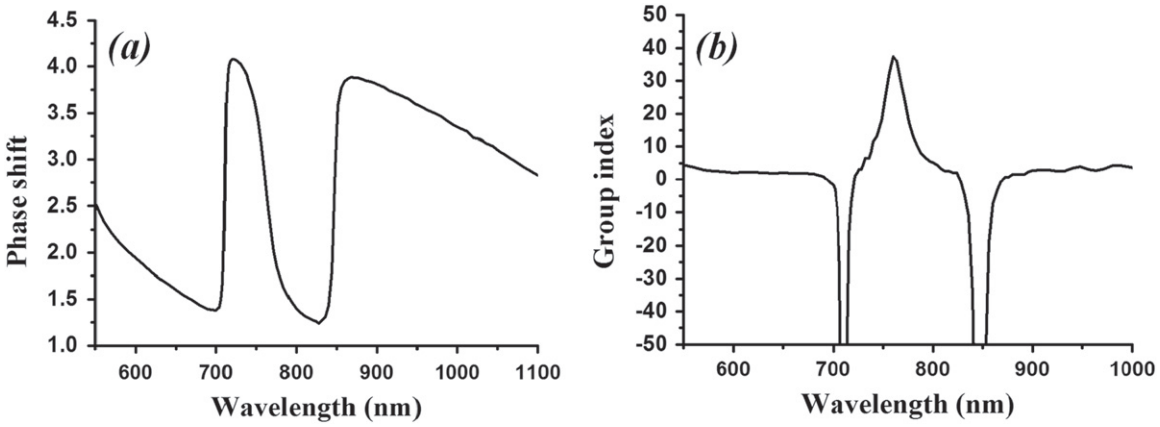

Figure 4. (a) The transmission phase shift and (b) group indices in the PIT system with $L = 500$ nm, $d = 100$ nm, $w = 50$ nm, $g = 10$ nm.

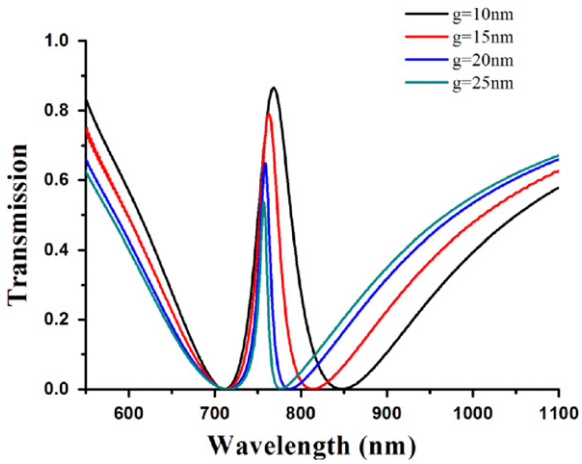

Figure 5. The transmission spectra for the coupled PIT system with different coupling gap size g ($L = 500$ nm, $d = 100$ nm).

size. And when coupling gap size decreases, the bandwidth of the PIT increases due to the enlarged energy gap between the two split resonant modes. Also, the blue shift of the split high energy resonant mode is much smaller than the red shift of the low energy resonant mode. The reason is that, except for the mode splitting mentioned above, the mode effective index in the gap region is increased with decreasing coupling gap size, which will induce red shifts of the resonances. Combing these two effects of the coupling gap size, the blue shift of the high energy mode is partly canceled while the red shift of the low energy mode is enhanced, which results in the above phenomenon.

Because the PIT is caused by the evanescent coupling between the MIM FP and MIM stub resonators, the resonant wavelength of the PIT peak can be adjusted by varying the lengths of MIM FP and MIM stub resonators, which changes the resonant wavelengths of the individual resonators. First, the effect of the MIM FP resonator length L on the transmission spectra is investigated and the obtained contour plot is shown in figure 6. In the wavelength range from 500 nm to 1200 nm, three PIT peaks can be observed by changing the MIM FP resonator length

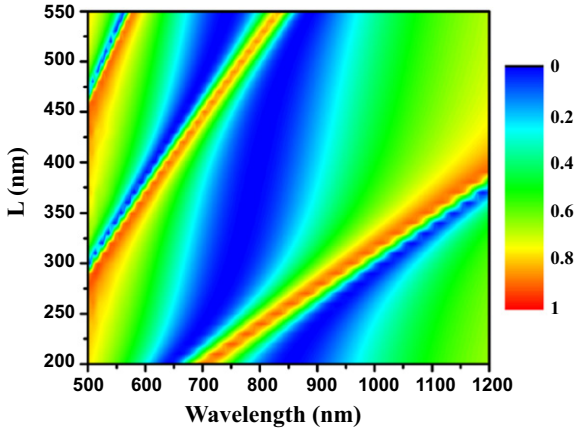

Figure 6. The contour plot of the transmission spectra with different MIM FP resonator lengths ($d = 100$ nm, $g = 10$ nm).

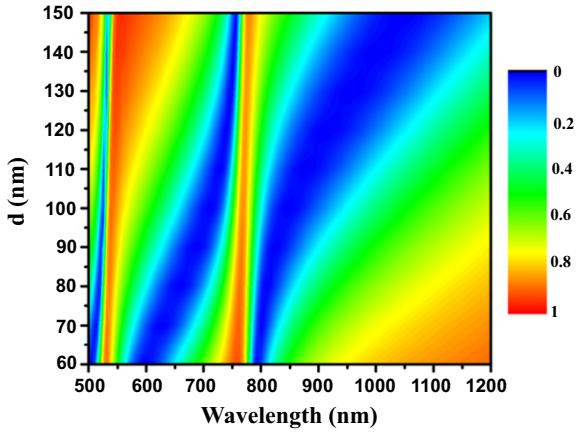

Figure 7. The contour plot of the transmission spectra with different MIM stub sizes ($L = 500$ nm, $g = 10$ nm).

L from 200 nm to 550 nm. Form the bottom to the top in figure 6, They are induced by the first-, second- and third-order resonances of the MIM FP resonator which interfere with the MIM stub resonator, respectively. And because the resonance band of the MIM stub resonator is broad, double PIT peaks can be obtained in occasions when the first and second order or second and third MIM FP resonances overlap with the MIM stub resonance. Also, it should be noted that the resonance wavelengths of the PIT peaks can be adjusted linearly by changing the MIM FP lengths, which can be useful in the applications.

Then the effect of the MIM stub length d on the transmission spectra is studied and the obtained contour plot is show in figure 7. Also, there are two PIT peaks in the wavelength range of 500 nm to 1200 nm. The PIT peaks around 750 nm and 540 nm are induced by the second and third MIM FP resonances, which interfere with the MIM stub resonance. From figure 6 and figure 7, comparing to the MIM FP length, the PIT resonant wavelength is much less sensitive to the MIM stub length. So the resonant wavelength mainly relies on the MIM FP resonator, whose resonant band is much narrower than that of the MIM stub.

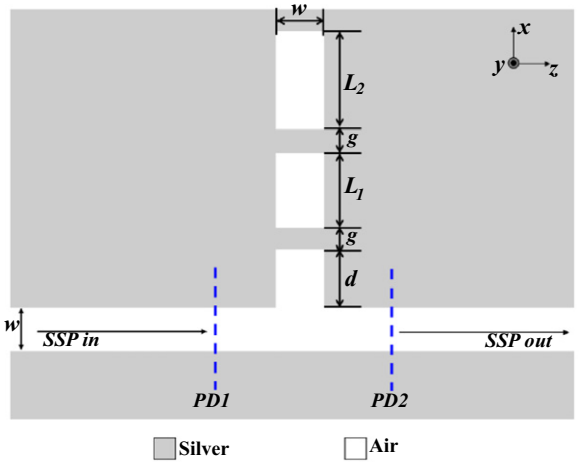

Figure 8. The schematic of the double PIT system with MIM stub coupled with double MIM FP resonator.

3. Double PIT induced by double FP resonators coupled with stub

The proposed PIT structure is flexible and can be easily extended to a double PIT system by adding another MIM FP resonator, as shown in figure 8. According to the resonant mode splitting due to the plasmon hybridization, double PIT peaks can be formed as the black dots shown in figure 9(a). Also the band stop spectra of the individual MIM FP resonators and the MIM stub resonator are shown as the blue line, green line and red line, respectively. And the magnetic field components H_y at the resonant dips and peaks are shown in figures 9(b)–(f). The H_y field distributions at the PIT peaks are shown in figure 9(c) and figure 9(e), where the MIM stub resonates weakly while the two MIM FPs resonate strongly, which is similar to the single PIT system. And the H_y fields in the two MIM FP resonators are inphase and antiphase for the high energy PIT peak and low energy PIT peak, respectively. Also, the H_y field in the MIM stub oscillates inphase with the H_y field of the input MIM waveguide, which induces the PIT phenomenon. On the contrary, when at resonant dips as shown in figure 9(b), figure 9(d) and figure 9(f), the H_y fields in the MIM stub are well coupled and oscillate antiphase with the H_y field of the input MIM waveguide, which can cause the destructive interferences and transmission dips.

Finally, the resonant wavelengths of the PIT peaks can be adjusted by altering the cavity length of the MIM FP resonator. Figure 10 shows the contour plot of the transmission spectra of the double PIT system with different MIM FP resonator length L_2 while keeping L_1 and d constants. Several phenomena can be observed: First, the two PIT peaks are both red shifted by increasing L_2 which is due to the red shift of the enlarging MIM FP cavity length; second, the resonant wavelengths of both PIT peaks are not linear with respective to the MIM FP cavity length L_2, which is different from the single PIT system, as shown in figure 6. This is caused by the energy gap induced by the mode splitting between the two evanescent coupled MIM FP resonators. And the smallest energy gap occurs when the two MIM FP resonators are the same length (here is $L_1 = L_2 = 500$ nm); third, by increasing the MIM FP cavity length L_2 from 400 nm to 600 nm, the high energy PIT peak gets stronger while the low energy PIT peak gets weaker. This phenomenon can be explained qualitatively as follows. The double PIT system can be

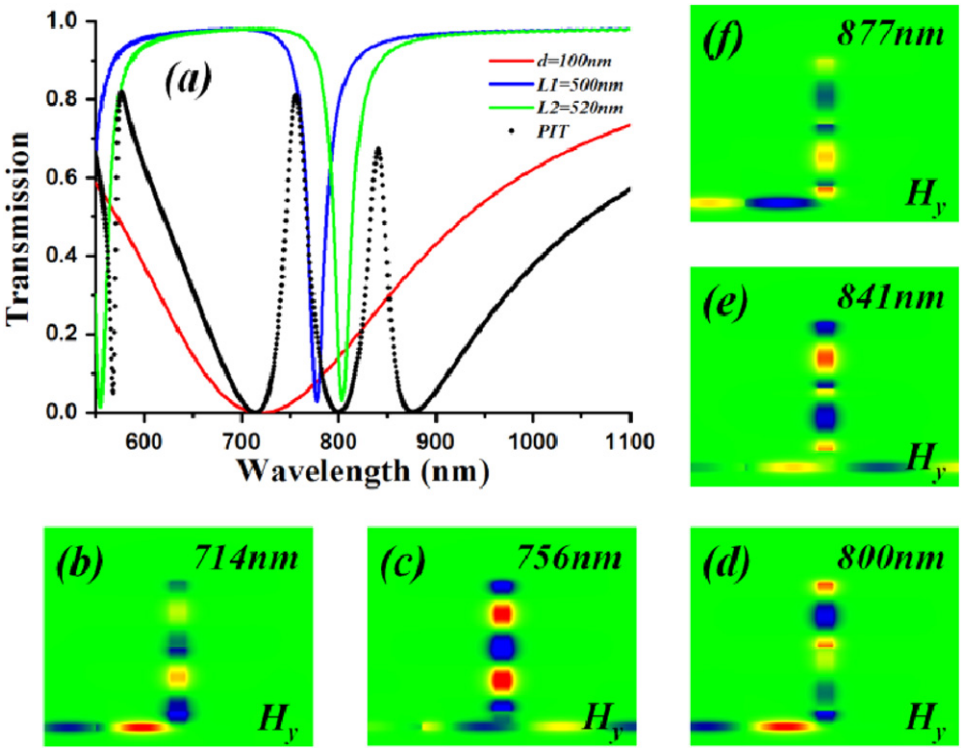

Figure 9. The transmission spectra of the individual MIM FP resonator ($L_1 = 500$ nm, blue line; $L_2 = 520$ nm, green line), stub (red line) and coupled PIT system (black dot); (b)–(f) The H_y field distributions of the coupled PIT system at resonant dips and peaks.

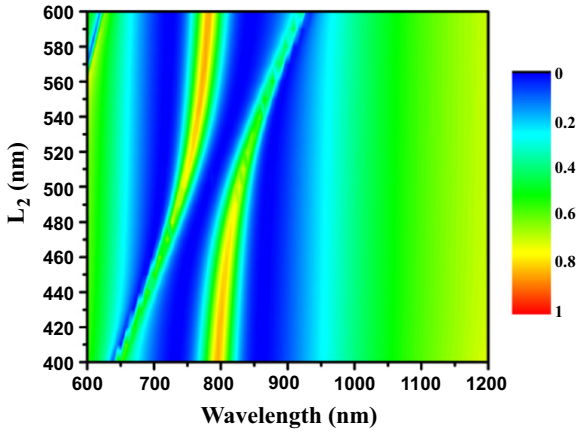

Figure 10. The contour plot of the transmission spectra with different MIM FP resonator lengths L_2 ($d = 100$ nm, $L_1 = 500$ nm, $g = 10$ nm).

regarded as a coupled system with three resonators: MIM stub, MIM FP_1 and MIM FP_2. Form figure 2(a), it is clear that the PIT peak induced by the MIM stub and MIM FP_1 is around 768 nm. When $L_2 = 400$ nm, the resonance wavelength of the MIM FP2 is much shorter than those of the MIM stub and MIM FP_1, so MIM stub and MIM FP_1 are strongly coupled while the MIM FP_2 is weakly coupled. In other words, high energy PIT peak which is mainly determined

by the weak coupling between MIM stub and MIM FP_2 is much weaker than the low energy PIT peak, which is mainly determined by the strong coupling between MIM stub and MIM FP_1. When the length of MIM FP_2 (L_2) increases, the resonance wavelength of MIM FP_2 increases and coupling between MIM FP_2 and MIM stub gets stronger, which enhances the low energy PIT peak. Also, the coupling between the MIM FP_1 and MIM FP_2 gets stronger, which causes the red shift and weakening of the low energy PIT peak due to the increased resonance wavelength mismatch between the MIM FP_1 and MIM stub. When $L_2 = L_1 = 500$ nm, the well-known anticrossing effect occurs by the strong coupling between the MIM FP_1 and MIM FP_2. When $L_2 > 500$ nm and increases, the coupling between MIM FP_2 an MIM stub is getting weaker due to the increased resonance wavelength mismatch between the MIM FP_2 and MIM stub, which causes the weakening of the low energy PIT peak.

4. Conclusion

A simple and compact plasmonic waveguide PIT system which includes a MIM stub evanescent coupled with a MIM FP resonator is proposed and analyzed. According to the plasmon hybridization theory, mode splitting can be caused by the evanescent coupling between the MIM stub and MIM FP resonators, which results in a high energy dip and a low energy dip in the PIT spectrum. The results show that when PIT occurs, the MIM FP resonates strongly while the MIM stub resonates weakly and oscillates inphase with respect to the input MIM waveguide. At the two split transmission dips, the MIM stub resonates strongly and oscillates antiphase with respect to the input MIM waveguide, which induces the destructive interferences. The resonant wavelength of the PIT system can be adjusted by altering the MIM FP resonator length. And the PIT peak strength can be increased by reducing the coupling gap size. Also, the proposed PIT structure can be easily extended to double PIT system by simply adding another MIM FP resonator.

Acknowledgments

This work was supported by the National Science Foundation of China under Grant No.60907025, No.11374048 and the Fundamental Research Funds for the Central Universities.

References:

[1] Ozbay E 2006 *Science* **311** 189
[2] Bozhevolnyi S I, Volkov V S, Devaux E, Laluet J-Y and Ebbesen T W 2006 *Nature* **440** 508
[3] Fleischhauer M, Imamoglu A and Marangos J P 2005 *Rev. Mod. Phys.* **77** 633
[4] Smith D D, Chang H, Fuller K A, Rosenberger A T and Boyd R W 2004 *Phys. Rev.* A **69** 063804
[5] Waks E and Vuckovic J 2006 *Phy. Rev. Lett.* **96** 153601
[6] Xu Q, Sandhu S, Povinelli M L, Shakya J, Fan S and Lipson M 2006 *Phys. Rev. Lett.* **96** 123901
[7] Kekatpure R D, Barnard E S, Cai W and Brongersma M L 2010 *Phys. Rev. Lett.* **104** 243902
[8] Yingran H, Hao Z, Yi J and Sailing H 2011 *Appl. Phys. Lett.* **99** 43113
[9] Chen J, Li Z, Zou Y, Deng Z, Xiao J and Gong Q 2013 *Plasmonics* **8** 1627
[10] Wang G, Lu H and Liu X 2012 *Opt. Express* **20** 20902
[11] Chen J, Li Z, Li J and Gong Q 2011 *Opt. Express* **19** 9976
[12] Huang Y, Min C and Veronis G 2011 *Appl. Phys. Lett.* **99** 143117

[13] Han Z and Bozhevolnyi S I 2011 *Opt. Express* **19** 3251
[14] Lu H, Liu X, Mao D, Gong Y and Wang G 2011 *Opt. Lett.* **36** 3233
[15] Yun B, Hu G and Cui Y 2013 *Opt. Commun.* **305** 17
[16] Lin X and Huang X 2008 *Opt. Lett.* **33** 2874
[17] Tao J, Huang X and Liu S 2010 *J. Opt. Soc. Am.* B **27** 1430
[18] Wang G, Lu H, Liu X and Gong Y 2012 *Nanotechnology* **23** 444009
[19] Cui Y and Zeng C 2013 *Opt. Commun.* **297** 190
[20] Yun B, Hu G and Cui Y 2011 *Opt. Commun.* **284** 485
[21] Liu L, Hao X, Ye Y, Liu J, Chen Z, Song Y, Luo Y, Zhang J and Tan L 2012 *Opt. Commun.* **285** 2558
[22] Chen J, Wang C, Zhang R and Xiao J 2012 *Opt. Lett.* **37** 5133
[23] Nordlander P, Oubre C, Prodan E, Li K and Stockman M I 2004 *Nano Lett.* **5** 899
[24] Lu H, Liu X and Mao D 2012 *Phys. Rev.* A **85** 053803
[25] Wang G, Lu H and Liu X 2012 *Appl. Phys. Lett.* **101** 013111